

Heat Transfer of Impinging Seawater Spray and Ice Accumulation on Marine Vessel Surfaces

A.R. Dehghani-Sanij*, G.F. Naterer, Y.S. Muzychka

Department of Mechanical Engineering, Faculty of Engineering and Applied Science,
Memorial University of Newfoundland, St. John's, NL, A1B 3X5, Canada

Abstract

In this paper, a new predictive model for the ice layer and water film growth, which occurs due to seawater spray impinging on large horizontal surfaces of a supply vessel, is developed using a Stefan-type problem formulation. The icing model includes conduction heat transfer in the ice and brine film layer, assuming the volume and distribution of brine pockets and air bubbles within the ice accumulation are uniform. The model also uses heat and mass balances to predict the freezing fraction, temperature distribution, ice layer and water film thickness. The results show that the water film salinity and icing intensity change with time during the icing period. Additionally, the water film salinity variations affect the freezing temperature, thermal conductivity and specific heat capacity of ice formation. As a result, heat conduction within the accumulated ice changes with time due to the variations of salinity; thus, the conduction heat flux has a significant effect on the ice thickness growth rate. This new model is a useful tool for forecasting and assessing the potential ice accumulation on marine vessels and structures.

Keywords: Heat transfer, Stefan problem, Sea spray icing, Ice accumulation, Cold seas and ocean regions

Nomenclature

a	Linearization constant, K^3
B_s	Shape coefficient, -
b	Ice layer thickness, m
C_d	Droplet drag coefficient, -
c_a	Specific heat capacity of air, $J/kg.K$
c_b	Specific heat capacity of brine, $J/kg.K$
c_i	Specific heat capacity of ice, $J/kg.K$
c_w	Specific heat capacity of seawater, $J/kg.K$
D	Water droplet diameter, m

* Corresponding author. PhD candidate, Department of Mechanical Engineering. E-mail address: adehghani@mun.ca

D_{ab}	Air-water vapour diffusivity, m^2/s
E	Collision efficiency, -
$e_s(T)$	Saturated vapour pressure, Pa
f_s	Slip factor, -
g	Gravitational acceleration, m/s^2
H_{bow}	Height of vessel bow above surface level, m
H_m	Maximum height of the spray jet, m
h	Height, m
h_c	Convection heat transfer coefficient, $W/m^2.K$
h_s	Significant wave height, m
k	Von Kármán constant, -
k_a	Thermal conductivity of air, $W/m.K$
k_b	Thermal conductivity of brine, $W/m.K$
k_i	Thermal conductivity of ice, $W/m.K$
L	Characteristic length, m
l_f	Latent heat of fusion of pure ice, J/kg
l_v	Latent heat of vaporization of water, J/kg
$\dot{M}_{evap,w}$	Mass flux of evaporation from brine film, $kg/m^2.s$
\dot{M}_{ice}	Mass flux of ice formation, $kg/m^2.s$
\dot{M}_{water}	Mass flux of brine film on the ice layer, $kg/m^2.s$
$\dot{M}_{w,t}$	Total mass flux of seawater spray, $kg/m^2.s$
n	Freezing fraction, -
P	Atmospheric pressure, Pa
Pr	Prandtl number
Q	Heat flux, W/m^2
Re	Reynolds number, -
RH	Relative humidity of air, %
r	Droplet radius, m
Sc	Schmidt number, -
S_b	Brine salinity, ppt
S_i	Ice salinity, ppt
S_w	Seawater salinity, ppt

T	Temperature, K
T_a	Temperature of air, K
T_b	Temperature of brine, $^{\circ}C$
T_d	Temperature of droplets, K
T_f	Freezing temperature of the water film at the water-ice interface, $^{\circ}C$
T_i	Temperature in the ice layer, K
T_s	Temperature of the water film at the air-water interface, $^{\circ}C$
T_w	Temperature in the water film, K
$T_{w,i}$	Temperature of seawater, K
t	Time, s
U	Wind velocity, m/s
U_h	Droplet velocity at the moment of impact on the plate, m/s
U_{10}	Wind velocity at a height of 10 m above mean sea level, m/s
u^*	Friction velocity, m/s
v_d	Droplet velocity, m/s
v_s	Vessel speed, m/s
v_{sw}	Vessel speed relative to the waves, m/s
x	Horizontal distance of the plate from the vessel's bow, m
z	Height from the water surface, m

Greek symbols

α	Angle between vessel heading and wind/wave direction, $^{\circ}$
α_a	Thermal diffusivity of air, m^2/s
α_b	Thermal diffusivity of brine, m^2/s
α_i	Thermal diffusivity of ice, m^2/s
β	Interfacial distribution coefficient, -
γ	Angle between the direction of wind velocity and vessel speed, $^{\circ}$
ε	Ratio of molecular weights of water vapour and dry air, -
ν_a	Kinematic viscosity of air, m^2/s
μ_a	Viscosity of air, $Pa.s$
η	Water film thickness, m
ρ_a	Density of air, kg/m^3
ρ_b	Density of brine, kg/m^3

ρ_i	Density of ice, including entrapped brine and air, kg/m^3
ρ_w	Density of seawater, kg/m^3
σ	Stefan-Boltzmann constant, $W/m^2.K^4$
τ_s	Duration of sea spray event, s
τ_p	Period between sea spray events, s
τ_w	Significant wave period, s
ω	Liquid Water Content (LWC), kg/m^3

1. Introduction

Atmospheric precipitation and seawater spray are the two major causes of icing phenomena on marine vessels and structures in cold seas and ocean regions. Atmospheric icing is created by freezing freshwater such as rain, snow, hail and drizzle, with rime ice resulting from supercooled cloud or fog droplets, and hoar frost resulting from the deposition of water vapour directly as ice crystals (Ryerson, 2011). Marine icing, or sea spray icing, can be generated in two different ways, which are wave spray and wind spray. Wave spray occurs from the impingement of waves with the marine vessel or structure. In addition, wind spray occurs when the wind blows droplets off whitecaps from the water's surface. Figure 1 illustrates a typical sea spray icing event on a marine vessel.

The highest amount of seawater spray generally occurs up to 15-20 m over the water surface. Within these heights, sea spray creates almost 50% to 90% of the icing on marine vessels (Cammaert, 2013). Several parameters have an impact on a sea spray event which leads to ice accumulation: the size and design of marine vessels and structures, the size and distribution of droplets, wind velocity, air temperature, vessel speed, droplet temperature, salinity, sea or ocean conditions, and the angle between vessel heading and wind/wave direction (Cammaert, 2013; Dehghani-Sanij et al., 2017; Jørgensen, 1985). A number of past studies reported that sea spray is a significant source of the icing phenomenon in cold seas and ocean regions (Aksyutin, 1979; Brown and Roebber, 1985; Cammaert, 2013; Makkonen, 1984; Shekhtman, 1968; Shellard, 1974; Tabata et al., 1963; Zakrzewski, 1986, 1987). Sea spray icing happens more than 80% of the time of reported icing events on marine vessels and structures in freezing conditions (Aksyutin, 1979; Brown and Roebber, 1985; Shekhtman, 1968; Zakrzewski, 1987).

The modeling of atmospheric icing for freezing freshwater from precipitation, cloud droplets and wet snow was reviewed by Makkonen (2000). He studied several factors, such as collision efficiency, sticking efficiency and accretion efficiency for the formation and growth of ice accumulation on structures. This study illustrates that the size

of droplets is one of the main factors for computing the collision efficiency. Furthermore, two forces affect a droplet during its flight above marine platforms: “aerodynamic drag” and “inertia”. As a result, the bigger droplets tend to collide with an obstacle because inertia forces are larger compared to the drag forces; the droplets also do not deflect significantly. Ryerson and Gow (2000) surveyed and estimated the properties of seawater spray and the conditions of weather and sea, as well as the amount of ice accumulation for sea spray icing on the vessel superstructures. This survey showed that: (1) the salinity of seawater was about 33‰ for two icing events (Ryerson, 1995); (2) by measuring approximately 7,000 droplets over 39 spray events, the range of droplet diameters was from 14 to 7700 μm (Ryerson, 1995); (3) the mean median volume diameter for all 39 spray events was 1094 μm , in the range of 169 to 6097 μm for single spray events (Ryerson and Gow, 2000); (4) the most severe icing on the trawler vessels occurs when wind velocities are larger than 20.6 m/s (Borisenkov and Panov, 1972); (5) when the temperature of air is less than $-5.0^{\circ}C$ and the velocity of wind is high, the temperature of seawater does not have a significant effect on the icing rate (Jørgensen, 1982).

Zakrzewski (1987) developed an improved model to determine the vertical distribution of the liquid water content (LWC) for wave-induced spray during the spray event. This formula was obtained based on Russian field data from the Sea of Japan. Furthermore, He calculated the time-averaged seawater spray flux for the components placed on the marine vessels. The time-averaged spray could be estimated for every specified wind velocity, fetch, vessel speed and heading angle. The observed results demonstrated that the seawater spray flux proliferates with wind velocity, vessel speed, and vessel heading. However, for a vessel heading of 90° , vessel speed does not affect the seawater spray flux. Moreover, seawater spray flux on large vertical plates was larger than on the cylindrical components for marine structures and vessels. Jones and Andreas (2012) provided two empirical correlations to compute wind spray droplet concentrations close to the ocean or sea surface for wind velocities from 0 to 28.8 m/s . These empirical correlations are functions of the droplet radius and U_{10} , which is the wind velocity at a height of 10 m above mean sea level. To calculate the vertical distribution of the LWC for the wind-induced spray, this model gives more accurate results. To determine the salinity of the accumulated ice layer and water film, Makkonen (1987) and Horjen (1990) developed an algebraic relationship for a stationary icing model. The evaporative mass flux was included in the model of Horjen (1990). In addition, Makkonen (1987) presented an explicit relationship for the freezing temperature of the brine as a function of salinity during phase equilibrium conditions.

The fundamentals of sea spray icing on marine vessels and structures were reviewed by Dehghani-Sanij et al. (2017). The processes and models of droplet trajectories, mass flux of sea spray, liquid water content (LWC), heat balance at the phase interface, and freezing equations were studied. These are key aspects to predict the icing rate and the quantity of the accumulated ice on marine platforms in cold seas and ocean regions. Myers and Hammond (1999) theoretically investigated a one-dimensional model for the growth of the ice layer and water film through impinging supercooled water droplets by analyzing the Stefan problem. To compute the ice layer and water film thicknesses, they used mass and heat balances as well as a phase change condition. In this study, two distinct boundary conditions, including a cooling condition and fixed temperature at the substrate, are employed. This study also analyzes and obtains the temperature distribution in the ice layer and water film. In another investigation, Brakel et al. (2007) studied and developed a one-dimensional model for the growth of ice accumulation by incoming supercooled droplets using an asymptotic analysis and a numerical method. They considered both dry- and wet- growth icing in this study. The results showed that there is a good agreement between the numerical model and asymptotic solution.

The main objective of this paper is to develop a new model to predict the freezing fraction, temperature distribution, and ice layer and water film thicknesses on horizontal icing surfaces of marine vessels and offshore structures involving seawater. Sea spray icing on a horizontal surface of marine platforms is analyzed with heat conduction in the ice and brine film calculated from the solution of a one-dimensional Stefan problem. The results are compared with other models for validation and verification purposes.

2. Model formulation

The prediction and assessment of the icing rate and the quantity of ice accumulation on marine platforms is a challenging and complex problem, because marine weather conditions change substantially. Some researchers have made different assumptions to compute the growth rate of ice on marine vessels and structures by various theoretical and numerical methods. One of these assumptions is to neglect atmospheric icing, since freezing owing to sea spray is the main cause of icing phenomena in cold seas and ocean regions (Aksyutin, 1979; Brown and Roebber, 1985; Cammaert, 2013; Makkonen, 1984; US Navy, 1988; Shekhtman, 1968; Shellard, 1974; Tabata et al., 1963; Zakrzewski, 1986, 1987). Another common assumption is that wave spray is regarded as being periodic for sea spray events. To predict and analyze the icing phenomenon on horizontal surfaces of marine platforms, a typical horizontal plate from the superstructure of a supply vessel is investigated. Figure 2 shows a schematic of the proposed problem with associated heat fluxes. Beyond for the estimation of the growth rate of ice on marine platforms, the calculation of

the trajectory of droplets is an important issue in the icing phenomena. Also, the position and orientation of surfaces that are located on marine vessels and structures play a considerable role in icing.

2.1. Droplet Trajectory

To determine the trajectory and velocity of the water droplets upon impact on marine platforms, several forces should be considered: air drag, gravity, and body forces (Dehghani et al., 2016a, 2016b; Fu et al., 2006; Kulyakhtin and Tsarau, 2014; Kulyakhtin et al., 2014; Lozowski et al., 2000; Lorenzini and Saro, 2013; Macdonald and McCartney, 1987; Makkonen, 2000). The motion of the droplets is governed by (Lozowski et al., 2000):

$$\frac{dv_d}{dt} = -\frac{3}{4} \frac{C_d \rho_a}{D \rho_d} |v_d - U| (v_d - U) - g \left(\frac{\rho_d}{\rho_a} - 1 \right) \quad (1)$$

In this equation, v_d , t , C_d , D , ρ_a , ρ_d , g and U are the droplet velocity, time, drag coefficient, droplet diameter, air density, droplet density (assumed to be equal to the density of seawater), gravitational acceleration, and wind velocity, respectively. The drag coefficient of the droplet, C_d , can be computed by (Langmuir and Blodgett, 1946; Lozowski et al., 2000):

$$C_d = \frac{24.0}{Re} + \frac{4.73}{Re^{0.37}} + 6.24 \times 10^{-3} Re^{0.38} \quad (2)$$

where Re is the Reynolds number of the droplet. The parameter of Re is given by:

$$Re = \frac{D}{\nu_a} |v_d - U| \quad (3)$$

where ν_a is the air kinematic viscosity. According to Dehghani et al. (2016b), the initial droplet velocity is equal to 47.14 m/s. The droplet velocity can be defined by combining Eqs. (1) to (3) and solving these equations using a numerical time stepping technique.

2.2. Sea spray impingement

As mentioned previously, sea spray has two principal but distinct sources, which are wave-induced spray and wind-induced spray. Wave spray is generally a major source of icing: it is mostly a concise and periodic water flux that is generated near the bow of vessels and the base of offshore structures. Also, wind spray is another (minor) source, but it is a constant water flux that is generated in the airstream in windy conditions (Dehghani-Sanij et al., 2015, 2017; Schröder Hansen, 2012).

The total mass flux of seawater spray, $\dot{M}_{w,t}$, during a spray event can be computed by:

$$\dot{M}_{w,t} = \dot{M}_{w,wind} + \dot{M}_{w,wave} \quad (t < \tau_s) \quad (4)$$

where τ_s is the duration of the spray event. The amount of the total mass flux of seawater spray on a flat plate per unit area and unit time for wind spray and wave spray is obtained by (Horjen, 1983; Zakrzewski, 1987):

$$\dot{M}_{w,t} = B_s E U_h [\omega(z)_{wind} + \omega(z)_{wave}] \quad (5)$$

where B_s is the shape coefficient, E is the collision efficiency, U_h is the droplet velocity at the moment of impact on the plate, and ω is the LWC. The collision efficiency for a horizontal plate can be considered equal to 1.

The LWC is a measure of the mass of water in a cloud in a determined amount of dry air. The LWC of the wind spray is written as follows (Jones and Andreas, 2012):

$$\frac{d\omega(r, z)}{dr} = \rho_w \left(\frac{4}{3} \pi r^3 \right) \left(\frac{z}{h} \right)^{-\frac{v_g(r)}{k u^* f_s}} \begin{cases} \frac{7 \times 10^4 U_{10}^2}{r} \exp \left(-\frac{1}{2} \left[\frac{\ln(r/0.3)}{\ln 2.8} \right]^2 \right), & \text{if } U_{10} < 19 \text{ m/s} \\ \frac{30 U_{10}^4}{r} \exp \left(-\frac{1}{2} \left[\frac{\ln(r/0.3)}{\ln 4} \right]^2 \right), & \text{if } U_{10} \geq 19 \text{ m/s} \end{cases} \quad (6)$$

where ρ_w is the density of seawater, k is the Von Kármán constant, f_s is the slip factor, u^* is the friction velocity, and h is the height, which is specified as the upper limit of the source region for spray droplet generation. For $U_{10} < 19 \text{ m/s}$, $h = 1 \text{ m}$ and for $U_{10} \geq 19 \text{ m/s}$, $h = 0.5 h_s$ where h_s is the wave height. The function $v_g(r)$ is the terminal velocity of the droplets. Then, the vertical distribution of the LWC of the wind spray can be written as:

$$\omega(z)_{wind} = \int_{r_{min}}^{r_{max}} E \frac{d\omega(r, z)}{dr} dr \quad (7)$$

If $U_{10} < 19 \text{ m/s}$, the maximum droplet radius assumed to contribute to icing is $100 \mu\text{m}$ and if $U_{10} \geq 19 \text{ m/s}$, it is $200 \mu\text{m}$. The minimum droplet radius assumed to contribute to icing is $5 \mu\text{m}$ (Jones and Andreas, 2012).

The vertical distribution of the LWC of the wave spray in the seawater spray event is expressed by the following formula (Zakrzewski, 1987):

$$\omega(z)_{wave} = 6.1457 \times 10^{-5} h_s v_{sw}^2 \exp \left(-\frac{(z - H_{bow})}{1.82} \right) \quad (8)$$

where H_{bow} is the height of the bow above the surface level. This study will use a coordinate system where $z = 0$ at the water surface. The parameter of v_{sw} is the vessel speed relative to the waves, which is calculated from (Aksyutin, 1979):

$$v_{sw} = \frac{g}{2\pi} \tau_w + v_s \cos(\pi - \alpha) \quad (9)$$

Here τ_w is the significant wave period, g is the gravitational acceleration and α is the angle between the vessel heading and the wind/wave direction (the wind and wave direction are assumed to be equal in this study). The maximum height of the spray jet can be determined by (Lozowski et al., 2000):

$$H_m = h_s + \frac{v_{sw}^2}{2g} \quad (10)$$

The term $\frac{v_{sw}^2}{2g}$ is based on an assumption that the ejection velocity of the droplets is approximately equal to the vessel speed relative to the waves and also air drag on the water droplets in motion is negligible (Lozowski et al., 2000). Note that spray jets do not occur in every vessel-wave collision (Aksyutin, 1979; Lozowski et al., 2000; Panov, 1976).

The duration of a spray event is written as follows (Zakrzewski, 1987):

$$\tau_s = \frac{C v_{sw} h_s}{U_{10}^2} \quad (11)$$

Here, C is an experimental constant, which is dependent on the shape and size of the ship hull (Zakrzewski, 1987). Zakrzewski (1987) used C as equal to 20.62. Spray frequency is a major factor to determine wave spray icing. Zakrzewski (1987) reported that the spray jet is created by every second wave on a fishing trawler. According to Horjen (2015), the mechanism of spray generation varies between a marine vessel and semi-submersible drill rig.

Two experimental correlations are obtained to estimate the significant wave height and period based on several observations for Norwegian waters. To calculate h_s , the following empirical correlation is used (Horjen, 1990, 2013, 2015) based on Norwegian wave height data (Jørgensen, 1985):

$$h_s = 0.752 U_{10}^{0.723} \quad (12)$$

Also, for obtaining τ_w the correlation below is employed (Horjen, 1990, 2013, 2015):

$$\tau_w = 6.161 h_s^{0.252} \quad (13)$$

Horjen (2013, 2015) considered that both every significant and every second significant wave generate spray in the numerical works. The total time period between spray events is estimated by (Aksyutin, 1979; Lozowski et al., 2000):

$$\tau_p = \frac{g \tau_w^2}{2\pi v_{sw}} \quad (14)$$

This relation is based on the assumption that every significant wave encounter produces spray. The seawater spray mass flux against time during the sea spray events is shown in Fig. 3. Note that only the wind spray remains in-between sea spray events ($\dot{M}_{w,t} = \dot{M}_{w,wind}$, $\tau_s < t < \tau_p$). An average value for the seawater spray mass flux is assumed in the model calculations.

2.3. Mass fluxes

A mass balance is utilized to estimate the ice layer and water film thicknesses. The mechanism of the ice accumulation process occurs so that the sea spray mass flux is transferred by the relative wind velocity and collides with the surface. The water droplet impinges on the surface and cools until freezing. The portion that does actually freeze on impact is called the freezing fraction, n , and the remaining fraction ($1-n$) is brine film.

By employing a mass balance for a horizontal plate, this can be written as:

$$\dot{M}_{w,t} = \dot{M}_{ice} + \dot{M}_{water} + \dot{M}_{evap,w} \quad (15)$$

where \dot{M}_{ice} is the mass flux of ice formation on the plate, \dot{M}_{water} is the mass flux of water film on the ice accumulation layer and $\dot{M}_{evap,w}$ is the mass flux of evaporation from the brine film. Then \dot{M}_{ice} can be written as follows:

$$\dot{M}_{ice} = n \dot{M}_{w,t} = \rho_i \frac{db}{dt} \quad (16)$$

where n is the freezing fraction that is between 0 and 1, ρ_i is the density of ice accumulation, including entrapped brine and air, b is the ice layer thickness, and $\frac{db}{dt}$ is the time derivative of b . The mass flux of evaporation from the brine film, $\dot{M}_{evap,w}$ is assumed to be negligible (Myers and Charpin, 2004; Myers et al., 2002; Schröder Hansen, 2012). To compute \dot{M}_{water} , it can be written as follows:

$$\dot{M}_{water} = (1-n) \dot{M}_{w,t} = \rho_b \frac{d\eta}{dt} \quad (17)$$

where ρ_b is the density of brine, η is the water film thickness, and $\frac{d\eta}{dt}$ is the time derivative of η . Note that for dry-growth icing (rime), n is equal to 1, and for wet-growth icing (glaze), n is less than 1.

2.4. Heat fluxes

According to Fig. 2, there are several heat fluxes present in the icing process: convection or sensible heat flux (losing energy), Q_c ; evaporation (losing energy), Q_e ; heat capacity of the impinging water droplets (losing energy),

Q_d ; radiation (losing energy), Q_r ; kinetic energy of incoming droplets (gaining energy), Q_k ; aerodynamic heating (gaining energy), Q_v ; release of latent heat (gaining energy), Q_f ; and heat flux by conduction, Q_a . Note that Q_v is significant at the high speeds characteristic of aircraft flight and the Q_k is normally small (Lozowski et al., 1983); hence, these heat fluxes are omitted in this study. Additionally, the authors ignore the effect of water flow on heat balance; however, it has an impact on the heat balance.

Heat loss by convection with the surrounding air is obtained by:

$$Q_c = h_c (T_s - T_a) \quad (18)$$

where h_c is the heat transfer coefficient, T_s is the temperature of the water film at the air-water interface, and T_a is the air temperature. The heat transfer coefficient is specified by body geometry, length, Reynolds number and Prandtl number. For a flat plate (or for planar components) in a turbulent flow parallel to the surface, an average heat transfer coefficient over a length L can be expressed by (Rohsenow and Choi, 1961):

$$h_c = 0.037 \frac{k_a}{L} Pr^{0.33} Re^{0.8} \quad (19)$$

where k_a is the thermal conductivity of air, L is the characteristic length of the component, Pr is the Prandtl number for the airflow, and Re is the Reynolds number of the component, which is defined using the relative wind velocity and the characteristic length of the component ($Re = U_{rs} L / v_a$). The characteristic dimension is taken to be the maximum dimension along the direction of the relative wind for the planar components.

Heat loss by evaporation to the surrounding air is calculated as follows (Bergman et al., 2011):

$$Q_e = h_c \left(\frac{Pr}{Sc} \right)^{0.63} \frac{\varepsilon l_v}{P c_a} (e_s(T) - RH \cdot e_s(T_a)) = C (e_s(T) - RH \cdot e_s(T_a)) \quad (20)$$

Here Sc is the Schmidt Number, ε is the ratio of molecular weights of water vapour and dry air, P is the atmospheric air pressure, l_v is latent heat of vaporization of water at the surface temperature, c_a is the specific heat capacity of dry air at a constant pressure, RH is the relative humidity of air, and $e_s(T)$ is the saturated vapour pressure, which has been linearized by the following relation (Myers, 2001):

$$e_s(T) \approx E_0 + e_0 T \quad (21)$$

where $e_0 = 27.03 \text{ Pa/K}$ and $E_0 = -6803 \text{ Pa}$. The relation above is accurate to within 8% over the range from 257 to 73 K (Myers, 2001).

The heat capacity of the impinging water droplets to the equilibrium surface temperature is given from (Kulyakhtin and Tsarau, 2014),

$$Q_d = \dot{M}_{w,wave} c_w (T_s - T_{d,wave}) + \dot{M}_{w,wind} c_w (T_s - T_{d,wind}) \quad (22)$$

where c_w is the specific heat capacity of seawater, and $T_{d,wave}$ and $T_{d,wind}$ are the droplet temperatures of the wave spray and wind spray immediately prior to impingement, respectively. The water droplet diameters in the wind spray are usually small, measuring less than $100 \mu m$ (Kulyakhtin and Tsarau, 2014). Thus, the temperature of the droplets will generally reach the air temperature in less than $0.1 s$ (Andreas, 1990); hence, the authors considered $T_{d,wind} = T_a$ in this study. The temperature of the droplets in the wave spray is between the air temperature and seawater temperature, because the droplet diameters are mostly larger (1 to $2 mm$) (Kulyakhtin and Tsarau, 2014). To estimate the temperature of the droplets of wave spray, an iterative procedure will be developed based on the model of Stallabrass (1980).

The radiative heat flux is defined by the following formula (Bergman et al., 2011; Chung and Lozowski, 2010):

$$Q_r = \sigma a (T_s - T_a) \quad (23)$$

where σ is the Stefan-Boltzmann constant, and a is a linearization constant that linearly approximates the black body radiation heat exchange between the icing surface and the airflow, where the emissivity of both is taken to be one.

The latent heat flux due to the freezing of a certain fraction of the impinging water droplets can be obtained by (Horjen, 1990):

$$Q_f = l_f (1 - \beta) \dot{M}_{ice} = l_f \rho_i (1 - \beta) \frac{db}{dt} \quad (24)$$

where l_f is the latent heat of fusion of pure ice and $l_f (1 - \beta)$ is the latent heat of fusion of the saline ice accumulation (Makkonen, 1987). Also, β is the interfacial distribution coefficient at the interface of ice and brine, which can be determined as follows:

$$\beta = \frac{S_i}{S_b} \quad (25)$$

In the relationship above, S_i is the salinity of ice formation and S_b is the salinity of brine.

2.5. Salt concentration

The salinity of sea or ocean water is one of the most important factors in the growth rate of sea spray icing. According to Jørgensen (1982), icing begins at higher temperatures when salinities are lower (Ryerson and Gow,

2000). Generally, the range of seawater salinity is approximately 33‰ to 37‰ (HyperPhysics site). Further, seawater salinity is typically 35‰ in most marine areas (Marine science site). As a result, all water droplets that are generated by wind spray and wave spray are saline; hence, only a portion of the impinging water freezes after impacting on objects located on marine platforms, and the excess water remains on the icing surfaces.

According to Makkonen (1987) and Szilder et al. (1995), during the freezing of a water film with a salinity of S_b , the ice formation can entrap only a part of the salt, namely βS_b , and the remainder will be rejected in the solution. Therefore, the salinity of the water film is related to the freezing temperature as follows (Schwerdtfeger, 1963):

$$S_b = \begin{cases} -0.0182 T_f, & \text{if } 0^\circ\text{C} \geq T_f > -8.2^\circ\text{C} \\ 0.149 - 0.01(T_f + 8.2), & \text{if } -8.2^\circ\text{C} \geq T_f > -23^\circ\text{C} \end{cases} \quad (26)$$

where T_f is the freezing temperature in units of $^\circ\text{C}$. In Eq. (26), the absolute value of brine salinity is used. Kulyakhtin and Tsarau (2014) expressed that when the brine temperature goes down to -23°C , the water, with all the salt included in it, will freeze.

Based on studies conducted by Horjen (2013, 2015), to calculate the salinity of the water film for a stationary icing model with no convective movement of the brine film is adopted by the following formula:

$$S_b = \frac{\dot{M}_{water} S_w}{\dot{M}_{water} + \dot{M}_{evap.,w} + \frac{(Q_i + Q_i)}{l_f}} \quad (27)$$

where Q_i is the conduction heat flux through the ice formation layer at the water-ice interface and Q_i is the net heat flux in the brine film at the air-water interface, which is equal to (Horjen, 2013):

$$Q_i = Q_c + Q_e + Q_d + Q_r \quad (28)$$

By neglecting $\dot{M}_{evap.,w}$ and from Eq. (24) and Eq. (27), after simplification, the following formula can be obtained.

$$S_b = \frac{I}{I - (1 - \beta)n} S_w \quad (29)$$

In the equation above, n is the freezing fraction. According to Makkonen (1987), the temperature of the water film at the air-water interface can be calculated by:

$$T_s = -54.0 S_b - 600 S_b^3 \quad (30)$$

Here, T_s is in units of $^\circ\text{C}$. In Eq. (30), the absolute amount of brine salinity is employed.

2.6. Heat transfer formulation

To predict and analyze the phenomenon of sea spray icing and the quantity of ice accumulation on the horizontal surfaces of marine platforms, a one-dimensional model will be used, as illustrated in Fig. 2. In this paper, conduction heat transfer through the ice layer is considered; also, the one-dimensional Stefan problem will be analyzed.

The governing equations for each layer are expressed by:

$$\frac{\partial}{\partial y} \left(k_b \frac{\partial T_w}{\partial y} \right) = \rho_b c_b \frac{\partial T_w}{\partial t}, \quad b \leq y \leq b + \eta \quad (31)$$

$$\frac{\partial}{\partial y} \left(k_i \frac{\partial T_i}{\partial y} \right) = \rho_i c_i \frac{\partial T_i}{\partial t}, \quad 0 \leq y \leq b \quad (32)$$

where T_w is the temperature in the water film, T_i is the temperature in the ice layer, k_b is the thermal conductivity of brine, k_i is the thermal conductivity of ice, ρ_b is the density of brine, ρ_i is the density of ice formation, c_b is the specific heat capacity of brine, and c_i is the specific heat capacity of ice accretion.

In the ice accumulation layer, pure ice, brine pockets and air bubbles exist (Blackmore et al., 2002; Makkonen, 1987). In reality, the volume and distribution of the brine pockets and air bubbles and the concentration of brine pockets in the ice layer are not uniform. As a result, the thermal conductivity, density, and specific heat capacity of ice accretion are a function of time, position and temperature. The ice formation can be called ‘‘spongy ice’’ (Makkonen, 1987). In this study, the authors assume that the volume and distribution of brine pockets and air bubbles and the concentration of the brine pockets within the accumulated ice are uniform. Thus, Eqs. (31) and (32) can be considered as follows:

$$\frac{\partial T_w}{\partial t} = \alpha_b \frac{\partial^2 T_w}{\partial y^2}, \quad \alpha_b = \frac{k_b}{\rho_b c_b}, \quad b \leq y \leq b + \eta \quad (33)$$

$$\frac{\partial T_i}{\partial t} = \alpha_i \frac{\partial^2 T_i}{\partial y^2}, \quad \alpha_i = \frac{k_i}{\rho_i c_i}, \quad 0 \leq y \leq b \quad (34)$$

where α_i and α_b are the thermal diffusivity of ice formation and brine, respectively. By using a phase change or Stefan condition at the ice-water interface, the following equation can be obtained:

$$\rho_i l_f (1 - \beta) \frac{db}{dt} = k_i \frac{\partial T_i}{\partial y} - k_b \frac{\partial T_w}{\partial y} \quad (35)$$

The equation above illustrates that the velocity of the interface is commensurate with the heat flux across it. To solve the problem, several boundary and initial conditions are needed, which are expressed as follows.

By applying the heat balance at the air-water interface, $b+\eta$, the equation below can be written as:

$$Q_{a,w} = Q_c + Q_e + Q_d + Q_r \quad (36)$$

where $Q_{a,w}$ is the heat conduction in the water film. By substituting Eqs. (18), (20), (22) and (23) into the above equation, the following relationship can be obtained.

$$\frac{dT_w}{dy} = A_w - B_w T_w(y, t), \quad y = b + \eta \quad (37)$$

where A_w and B_w are coefficients independent of the water film temperature. They are determined as:

$$A_w = \frac{[(h_c + C e_0 RH + \dot{M}_{w,wind} c_w + \sigma a) T_a + C E_0 (RH - 1) + \dot{M}_{w,wave} c_w T_{d,wave}]}{k_b} \quad (38)$$

$$B_w = \frac{[h_c + C e_0 + \dot{M}_{w,t} c_w + \sigma a]}{k_b} \quad (39)$$

For the ice-water interface, b , the ice accretion and brine are at the freezing temperature, T_f . Thus,

$$T_w(b, t) = T_i(b, t) = T_f \quad (40)$$

Also, at the surface between the ice and substrate, a constant temperature is considered. Therefore,

$$T_i(0, t) = T_{sub} \quad (41)$$

The initial conditions are given by:

$$\eta(0) = b(0) = 0, \quad t=0 \quad (42)$$

By considering a constant temperature below freezing at the substrate, the process of icing happens in two separate phases. In the first phase, all the impinged water droplets will freeze immediately, but in the second phase, both the water film and ice layer increase at the same time. During the first phase, when only ice accumulation is increasing, since the freezing fraction, n , is equal to 1, the thickness of the ice layer can be obtained by the following relationship:

$$b(t) = \frac{\dot{M}_{w,t}}{\rho_i} t \quad (43)$$

Non-dimensionalization of the heat equation for the ice layer is performed by taking the time-scale from Eq. (43), thereby yielding:

$$\frac{\partial^2 T_i^*}{\partial y^{*2}} = \lambda_i \frac{\partial T_i^*}{\partial t^*} \quad (44)$$

where

$$T^* = \frac{T - T_a}{T_f - T_a}, \quad y^* = \frac{y}{b}, \quad t^* = \left(\frac{\dot{M}_{w,t}}{\rho_i b} \right), \quad \lambda_i = \frac{c_i b^* \dot{M}_{w,t}}{k_i} \quad (45)$$

and

$$b^* \ll \frac{k_i}{c_i \dot{M}_{w,t}} \quad (46)$$

Here b^* is the non-dimensional height-scale. The right hand side of Eq. (44) is very small ($\lambda_i \ll 1$). Thus,

$$\frac{\partial^2 T_i^*}{\partial y^{*2}} \approx 0 \quad (47)$$

The dimensional form of the above equation can be written as:

$$\frac{\partial^2 T_i}{\partial y^2} \approx 0 \quad (48)$$

To solve Eq. (48) and obtain the temperature distribution in the ice layer, two boundary conditions are required. One of them is Eq. (41) and another, by employing the heat balance at the air-ice interface, is given by:

$$Q_{a,i} = Q_c + Q_e + Q_d + Q_r \quad (49)$$

where $Q_{a,i}$ is the heat conduction term in the ice layer. By substituting Eqs. (18), (20), (22) and (23) in Eq. (49), the following relationship can be obtained.

$$\frac{\partial T_i}{\partial y} = A_i - B_i T_i(y, t), \quad y = b \quad (50)$$

where the coefficients of A_i and B_i are defined as:

$$A_i = \frac{[(h_c + C e_0 RH + \dot{M}_{w,wind} c_w + \sigma a) T_a + C E_0 (RH - 1) + \dot{M}_{w,wave} c_w T_{d,wave}]}{k_i} \quad (51)$$

$$B_i = \frac{[h_c + C e_0 + \dot{M}_{w,t} c_w + \sigma a]}{k_i} \quad (52)$$

Then the temperature distribution in the ice layer is written as follows:

$$T_i = G y + T_{sub} \quad (53)$$

where G is a constant coefficient. Eq. (53) illustrates that the temperature profile is linear in y . These problems are called “quasi or pseudo-steady” (Myers and Hammond, 1999). Time enters through the moving boundary conditions, exerted at $y=b(t)$.

In the second phase, a water film increases on the surface of the ice layer. As in the previous phase, the energy equations, (33) and (34), can be simplified to quasi-steady forms. Thus,

$$\frac{d^2 T_i}{dy^2} \approx 0, \quad \frac{d^2 T_w}{dy^2} \approx 0 \quad (54)$$

while

$$b^* \ll \frac{k_i}{(1-\psi)c_i \dot{M}_{w,t}} \quad \& \quad \eta^* \ll \frac{k_b}{\psi c_b \dot{M}_{w,t}} \quad (55)$$

where ψ is the fraction of brine that stays liquid. The water film has to remain thin, unless there is a slow growth of water, $\psi \ll 1$, which permits time for the temperature to adjust.

The temperature distribution in the ice layer is given as follows:

$$T_i = \left(\frac{T_f - T_{sub}}{b} \right) y + T_{sub} \quad (56)$$

Also, the temperature distribution in the water film is equal to:

$$T_w = \left(\frac{A_w - B_w T_f}{I + B_w \eta} \right) (y - b) + T_f \quad (57)$$

In the water film, there is a temperature gradient. The temperature gradient will be large when the freezing fraction, n , is near 0, and will be small when the freezing fraction, n , is near 1. Note that during the icing conditions, there will be a turbulent mixture of the water film, so by considering the average value of the water film temperature, Eq. (57) will be more accurate.

By taking the derivative of Eqs. (56) and (57) and substituting these equations in the Stefan condition (Eq. (35)), the equation below will be obtained:

$$\rho_i l_f (I - \beta) \frac{db}{dt} = k_i \left(\frac{T_f - T_{sub}}{b} \right) - k_b \left(\frac{A_w - B_w T_f}{I + B_w \eta} \right) \quad (58)$$

This equation shows that several parameters have an impact on the growth rate of the icing on marine vessels and offshore structures. Some of the major parameters include: wind velocity, vessel speed, air temperature, seawater

salinity, height from the water surface, angle between vessel heading and wind/wave direction, droplet size, relative humidity, droplet temperature and time. By substituting Eq. (16) in Eq. (58), the following equation can be obtained:

$$l_f (1 - \beta) n \dot{M}_{w,t} - k_i \left(\frac{T_f - T_{sub}}{b} \right) + k_b \left(\frac{A_w - B_w T_f}{1 + B_w \eta} \right) = 0 \quad (59)$$

By solving the equation above, the freezing fraction, n , will be determined. For this purpose, the parameters of b , η , T_f and T_{sub} should be replaced in Eq. (59). The parameters of b and η are defined by integrating Eqs. (16) and (17), respectively. Also, the freezing temperature of brine film, T_f , can be calculated by Eq. (26). According to Myers and Charpin (2004), T_{sub} will usually be equal to the ambient temperature, T_a .

3. Results and discussion

To solve the algebraic equations and obtain the freezing fraction, temperature distribution, and the ice layer and water film thicknesses, several parameters and properties will be used. According to Cox and Weeks (1983) and Horjen (2013), the density of ice can be approximated by:

$$\rho_i = \begin{cases} \frac{(1 - v'_a)}{\frac{1}{\rho_{i,p}} - \beta \left(\frac{1}{\rho_{i,p}} - \frac{1}{\rho_b} \right)}, & S_b < 125\% \\ \frac{(1 - v'_a)}{\frac{1}{\rho_{i,p}} - \beta S_b \frac{P_3(T_b)}{Q_3(T_b)}}, & S_b \geq 125\% \end{cases} \quad (60)$$

where v'_a is the volume fraction of air in the ice (in this study considered equal to 0), $\rho_{i,p}$ is the density of pure ice ($\rho_{i,p} = 917 \text{ kg/m}^3$ (Brakel et al., 2007; Pringle et al., 2007)), ρ_b is the density of brine, T_b is the temperature of brine, and the parameters of $P_3(T_b)$ and $Q_3(T_b)$ are two third degree polynomials of the brine temperature, as follows (Cox and Weeks, 1983; Horjen, 2013):

$$\begin{cases} P_3(T_b) = 8.903 \times 10^{-2} - 1.763 \times 10^{-2} T_b - 5.33 \times 10^{-4} T_b^2 - 8.801 \times 10^{-6} T_b^3 \\ Q_3(T_b) = -4.732 \times 10^3 - 2.245 \times 10^4 T_b - 6.397 \times 10^2 T_b^2 - 10.74 T_b^3 \end{cases} \quad (61)$$

The temperature of brine, T_b , can be computed by (Assur, 1958):

$$T_b = -\frac{a S_b}{1 - 10^{-3} S_b}, \quad S_b < 125\% \quad (62)$$

$$T_b = -\frac{b S_b}{1 - 10^{-3} S_b} + c, \quad 125\% \leq S_b < 230\% \quad (63)$$

Here, $a = 5.4113 \times 10^{-2} \text{ }^\circ\text{C}$, $b = 9.7007 \times 10^{-2} \text{ }^\circ\text{C}$ and $c = 6.0533 \text{ }^\circ\text{C}$. The density of brine, ρ_b , is given by (Horjen, 2013):

$$\rho_b = 1000 + 0.8 S_b \quad (64)$$

The thermal conductivity of brine, k_b , can be calculated by (Lange and Forke, 1952; Pringle et al., 2007):

$$k_b = 0.523 + 0.013 T_b \quad (65)$$

The Prandtl number, Pr , and the Schmidt number, Sc , respectively, are given as:

$$Pr = \frac{\mu_a}{\rho_a \alpha_a} \quad (66)$$

$$Sc = \frac{\mu_a}{\rho_a D_{ab}} \quad (67)$$

Here μ_a is the air viscosity, α_a is the thermal diffusivity of air, and D_{ab} is the air-water vapour diffusivity. The dynamic viscosity of air, μ_a , is expressed by (Tracy et al., 1980):

$$\mu_a = \mu_o \left[\frac{T_o + C}{T + C} \left(\frac{T}{T_o} \right)^{1.5} \right] \quad (68)$$

where $\mu_o = 1.8325 \times 10^{-5}$, $T_o = 296.16$, $C = 120$ and $T = T_a + 273.15$. Also, the density of air is (Tracy et al., 1980):

$$\rho_a = \frac{P}{287.04(T_a + 273.15)} \quad (69)$$

In the formula above, P is the atmospheric air pressure and T_a (air temperature) is in units of $^\circ\text{C}$. The kinematic viscosity of air is given by:

$$v_a = \frac{\mu_a}{\rho_a} \quad (70)$$

The standard atmospheric pressure, P , can be written as follows (Tracy et al., 1980):

$$P = 101325 \left[1 - (2.2569 \times 10^{-5} z) \right]^{5.2553}, \quad -1000 < z < 2000 \text{ m} \quad (71)$$

where z is the height. The thermal conductivity of ice accumulation is dependent on the configuration of ice, which includes pure ice, brine pockets and air bubbles. Pringle et al. (2007) developed a model for estimating the thermal conductivity of ice by considering the first-order temperature dependence of the individual conductivities in the ice. Additionally, the authors neglected the conductivity of the air bubbles. This formula is written as follows:

$$k_i = \left(\frac{\rho_i}{\rho_{i,p}} \right) \left[2.11 - 0.011T + 0.09 \frac{S_i}{T} - \frac{(\rho_i - \rho_{i,p})}{1000} \right] \quad (72)$$

where S_i is the salinity of ice formation, T is the temperature in $^{\circ}C$ and the thermal conductivity is in units of W/mK . The above formula is based on a geometrical configuration of bubbly brine inclusions. Note that Fichet and Maqueda (1997) considered a constant thermal conductivity of sea ice equal to $2.03 W/mK$. The specific heat capacity of ice formation, c_i , can be determined by (Ono, 1967):

$$c_i = 0.505 + 0.0018T + 4.3115 \frac{S_i}{T^2} \quad (73)$$

In this relation, c_i , has units of $Cal/gr^{\circ}C$. To estimate the temperature in Eqs. (72) and (73), a temperature equal to T_f was assumed.

Other parameters in the modeling of the horizontal icing process are illustrated in Table 1. Figure 4 shows the droplet velocity changes during flight on a marine vessel when the average diameter of the water droplets is assumed equal to $1.5 mm$. As a result, the droplet velocity at initial times is very large. Then the droplet velocity will decrease until the terminal velocity is reached. Figure 5 indicates the freezing fraction changes with air temperature at three different times. As can be seen in this figure, when the air temperature goes below $-1.85^{\circ}C$ ($271.3 K$), ice accumulation begins. Tabata et al. (1963), Tabata (1969), Lundqvist and Udin (1977), and Cammaert (2013) showed that ice accretion will form on marine platforms once the air temperature is approximately $-2^{\circ}C$ ($271.15 K$). As a result from Fig. 5, with increasing time, freezing occurs at lower air temperatures; for instance, there is a lower air temperature for the freezing fraction equal to 1 when time increases. Thus, time has a considerable effect on the freezing fraction. Figure 6 illustrates the changes in the freezing fraction with time for several air temperatures. At initial times, water droplets will freeze quickly because the droplet collision adapts to the sub-zero substrate temperature, such that there is nearly dry-growth rime icing at air temperatures of $266 K$ and $264 K$. By increasing time, both the ice layer and brine film will grow simultaneously; however, with increasing time at a constant air temperature, the growth rate of ice accumulation is less than the brine film. Additionally, Fig. 6 shows that the amount of the freezing fraction at lower air temperatures is greater compared to higher air temperatures. Therefore, the air temperature is an important factor in increasing icing rates.

Figure 7 shows the changes of ice formation thickness with time for different air temperatures. As observed in this figure, with increasing time and decreasing air temperature, the thickness of ice accumulation will increase despite the

change of salinity in the ice layer. There is a feedback mechanism between the icing intensity and the brine film salinity, such that with increasing icing intensity, the brine film salinity will increase (Horjen, 2015); then, due to the increased salinity over time, the icing intensity will decrease. Additionally, salinity has a smaller impact on the freezing fraction at lower air temperatures. In other words, the icing intensity will increase at lower air temperatures. As described in Figs. 5-7, the parameters of time, air temperature, and salinity can play a significant role in the growth rate of ice on vessels and marine platforms.

Table 2 indicates the changes of air temperature and the thickness of ice accumulation at different times for dry-growth icing. Also, Table 3 displays the changes of the freezing fraction and the ice layer and water film thicknesses for wet-growth icing at $T_a=266.1\text{ K}$. Figure 8 shows and compares the changes of the ice layer and brine film thicknesses with time for two distinct conditions, which are expressed in Tables 2 and 3. According to Fig. 8 and Table 3, the thicknesses of the ice layer and water film, when time is equal to 5 min, are 1.057 mm and 0.064 mm, respectively. In other words, after impinging on the surface, the water droplets will freeze immediately at initial times (approximately less than 5 min); this is called the first phase. However, for the second phase, both the water film and ice layer increase at the same time, but the growth rate of these layers varies over time.

Figures 9 and 10 represent the influence of the seawater spray salinity and wind velocity, respectively, when the time is equal to 1 h. In these figures, the authors consider that one parameter is variable, while the other parameters are kept constant. According to Fig. 9, by decreasing the salinity, the freezing fraction is equal to 1 below higher air temperatures. As a result, the salinity affects several parameters, such as density, specific heat capacity and freezing temperature. When the wind velocity increases, the freezing fraction drops (Fig. 10), because the wind velocity has a significant effect on the total flux of seawater spray and convection, evaporation, and the heat capacity of the impinging droplets.

The authors compared the predicted results with past results reported by Dehghani-Sanij et al. (2016). A number of past studies assumed that conduction heat transfer inside the ice formation layer was negligible, and therefore neglected it (Dehghani-Sanij et al., 2016; Horjen, 1990, 2013, 2015; Kulyakhtin and Tsarau, 2014; Lozowski et al., 2000; Makkonen, 1987, 2010). Dehghani-Sanij et al. (2016) predicted the growth rate of icing and the quantity of ice accumulation on a horizontal surface of marine platforms. Figure 11 shows and compares the thicknesses of ice formation and water film for two different approaches with identical parameters. As illustrated in this figure, in the case that heat conduction is considered within the ice layer (solid line), by increasing time at a constant air

temperature (266.1 K), the rates of growth of ice formation and brine film are different. For comparison purposes, when the heat conduction is assumed negligible in the ice accretion (dash lines), and time increases at a constant air temperature, the rates of growth of both the ice layer and brine film are the same. As a result, the conductive heat flux inside the ice accumulation layer has a considerable effect on the growth rate of icing because of the changes of the water film salinity and the icing intensity over time.

4. Conclusions

A new predictive model was developed to analyze the icing process on horizontal surfaces of marine vessels and offshore structures in cold seas and ocean regions. In this paper, conduction heat transfer within the ice layer was considered. It was assumed that the volume and distribution of brine pockets and air bubbles inside the ice accumulation were uniform. The freezing fraction, temperature distribution, ice layer and water film thicknesses were predicted using heat and mass balances as well as phase change conditions. The results showed that the variations of air temperature, wind velocity, time, and salinity affect the growth rate of the ice formation on vessels and marine platforms. With the change of time, the water film salinity and the icing intensity will vary. By decreasing the air temperature, the icing intensity will increase. Moreover, the variations of water film salinity affect the thermal conductivity, the specific heat capacity of ice accumulation, and the freezing temperature. As a result, heat conduction within the accumulated ice layer has a substantial impact on the growth rate of icing of marine vessels and structures during the freezing conditions in cold seas and ocean regions.

Acknowledgements

The authors gratefully acknowledge the financial support from Statoil (Norway), the Research and Development Corporation of Newfoundland and Labrador (RDC), MITACS and the Petroleum Research of Newfoundland & Labrador (PRNL), and American Bureau of Shipping (ABS) Group for this study.

References

- Aksyutin, L.R., (1979). Icing of ships. *Sudostroeyne Publishing House*, Leningrad, (126 pp). (in Russian)
- Andreas, E.L., (1990). Time constants for the evolution of sea spray droplets. *Tellus B*, 42 (5), 481-497.
- Assur, A., (1958). Composition of sea ice and its tensile strength, Arctic Sea Ice. *US National Academic Sciences-National Research Council Pub.*, 598, 106-138.
- Bergman, T.L., Lavine, A.S., Incropera, F.P., and DeWitt, D.P., (2011). *Introduction to Heat Transfer*. 6th Edition, John Wiley & Sons, Inc.

- Blackmore, R.Z., Makkonen, L., and Lozowski, E.P., (2002). A new model of spongy icing from first principles. *Journal of Geophysical Research*, 107 (D21).
- Borisenkov, E.P., and Panov, V.V., (1972). Basic results and perspectives on the investigation of hydro meteorological conditions related to ship icing. (in Russian)
- Brakel, T.W., Charpin, J.P.F., and Myers, T.G., (2007). One-dimensional ice growth due to incoming supercooled droplets impacting on a thin conducting substrate. *Int. J. Heat Mass Transfer*, 50, 1694-1705.
- Brown, R.D., and Roebber, P., (1985). The ice accretion problem in Canadian waters related to offshore energy and transportation. *Canadian Climate Centre*. Report No. 85.13, Downsview, Ont., (295 pp).
- Cammaert, G., (2013). Impact of marine icing on Arctic offshore operations. *Pilot Project*, Volume 5 of Arctic Marine Operations Challenges & Recommendations Report.
- Chung, K.K., and Lozowski, E.P., (2010). On the growth of marine icicles. *Atmosphere-Ocean*, 28 (4), 393-408.
- Cox, G.F.N., and Weeks, W.F., (1983). Equations for determining the gas and brine volumes of sea-ice samples. *J. Glaciol.*, 29 (102), 306-316.
- Dehghani, S.R., Muzychka, Y.S., and Naterer, G.F., (2016a). Droplet trajectories of wave-impact sea spray on a marine vessel. *Cold Regi. Sci. Tech.*, 127, 1–9.
- Dehghani, S.R., Naterer, G.F., and Muzychka, Y.S., (2016b). Droplet size and velocity distributions of wave-impact sea spray over a marine vessel. *Cold Regi. Sci. Tech.*, 132, 60–67.
- Dehghani-Sanij, A.R., Muzychka, Y.S., and Naterer, G.F., (2015). Analysis of Ice Accretion on Vertical Surfaces of Marine Vessels and Structures in Arctic Conditions. *The ASME 2015 34th International Conference on Ocean, Offshore and Arctic Engineering (OMAE2015)*, OMAE2015-41306, St. John's, Newfoundland, Canada.
- Dehghani-Sanij, A.R., Muzychka, Y.S., and Naterer, G.F., (2016). Predicted Ice Accretion on Horizontal Surfaces of Marine Vessels and Offshore Structures in Arctic Regions. *The ASME 2015 35th International Conference on Ocean, Offshore and Arctic Engineering (OMAE2016)*, OMAE2016-54054, Busan, South Korea.
- Dehghani-Sanij, A.R., Dehghani, S.R., Naterer, G.F., and Muzychka, Y.S., (2017). Sea Spray Icing Phenomena on Marine Vessels and Offshore Structures: Review and Formulation, *Ocean Engineering*, 132, 25-39.
- Engineering Toolbox, 2016. Retrieved from: <http://www.engineeringtoolbox.com>
- Environment and Climate Change, Canada, Met 101. Retrieved from: <http://www.ec.gc.ca/meteo-weather/default.asp?lang=En&n=279AC7ED-1&offset=6&toc=show>

- Fichefet, T., and Maqueda, M.M., (1997). Sensitivity of a global sea ice model to the treatment of ice thermodynamics and dynamics. *J. Geophys. Res.*, 102 (12), 609-646.
- Fu, P., Farzaneh, M., and Bouchard, G., (2006). Two-Dimensional Modelling of the Ice Accretion Process on Transmission Line Wires and Conductors. *Cold Regi. Sci. Tech.*, 46, 132–146.
- Green, D.W., and Perry, R.H., (2008). *Perry's Chemical Engineers' Handbook*. 8th Edition, McGraw-Hill, New York, USA.
- Horjen, I., (1983). Mobile platform stability. *MOPS Subproject 02-Icing*, MOPS report No. 7, Norwegian Hydrodynamic Laboratories, NHL 283021.
- Horjen, I., (1990). Numerical modeling of time-dependent marine icing, anti-icing and deicing. *Doctoral thesis*, Norges Tekniske Høgskole (NTH), Trondheim, Norway.
- Horjen, I., (2013). Numerical modeling of two-dimensional sea spray icing on vessel-mounted cylinders. *Cold Regi. Sci. Tech.*, 93, 20-35.
- Horjen, I., (2015). Offshore drilling rig ice accretion modeling including a surficial brine film. *Cold Regi. Sci. Tech.*, 119, 84-110.
- HyperPhysics site, Department of Physics and Astronomy, Georgia State University, Atlanta, GA, USA. Retrieved from: <http://hyperphysics.phy-astr.gsu.edu/hbase/chemical/seawater.html>
- Jones, K.F., and Andreas, E.L., (2012). Sea spray concentrations and the icing of fixed offshore structures. *Q. J. R. Meteor. Soci.*, 138, 131-144.
- Jørgensen, T.S., (1982). Influence of ice accretion on activity in the northern part of the Norwegian continental shelf. *Offshore Technology Testing and Research report No. F82016*. Trondheim, Norway: Continental Shelf Institute, Norwegian Hydrodynamic Laboratories.
- Jørgensen, T.S., (1985). Impacts on safety and operation of marine units due to ice accretion. *J. Bull. Norwegian Hydrotech. Lab.*, pp. 79-84.
- Kato, R., (2012). Modeling of ship superstructure icing: application to ice bridge simulators. *MS thesis*, Department of Marine Technology, Norwegian University of Science and Technology, Norway.
- Kulyakhtin, A., and Tsarau, A., (2014). A time-dependent model of marine icing with application of computational fluid dynamics. *Cold Regi. Sci. Tech.*, 104-105, 33-44.

- Kulyakhtin, A., Shipilova, O., and Muskulus, M., 2014. Numerical Simulation of Droplet Impingement and Flow around a Cylinder Using RANS and LES. *J. Fluids Structure*, 48, 280–294.
- Lange, N.A., and Forke, G.M., 1952. *Handbook of chemistry*. 8th ed., Handbook Publ., Sandusky, Ohio.
- Lundqvist, J.E., and Udin, I., 1977. Ice accretion on ships with special emphasis on Baltic conditions. *Winter Navigation Research Board, Swedish Administration of Shipping and Navigation, Finnish Board of Navigation*, Research Report No. 23.
- Lorenzini, G., and Saro, O., (2013). Thermal Fluid Dynamic Modelling of Water Droplet Evaporation in Air. *Int. J. Heat Mass Transfer*, 62, 323–335.
- Lozowski, E.P., Szilder, K., and Makkonen, L., (2000). Computer simulation of marine ice accretion. *Royal Society of London Philosophical Transactions Series A*, 358, 2811-2845.
- Lozowski, E.P., Stallabrass, J.R., and Hearty, P.F., (1983). The icing of an unheated, non-rotating cylinder, Part I: a simulation model, *J. Climate Appl. Meteorology*, 22, 2053-2062.
- Macdonald, O.C., and McCartney, H.A., (1987). Calculation of splash droplet trajectories. *Agric. For. Meteorol.*, 39, 95-110.
- Makkonen, L., (1984). Atmospheric icing on sea structures. *US Army Cold Regions Research and Engineering Laboratory*, Monograph 84-2, Vol. 102.
- Makkonen, L., (1987). Salinity and growth of ice formed by sea spray. *Cold Regi. Sci. Tech.*, 14, 163-171.
- Makkonen, L., (1989). Estimation of wet snow accretion on structures. *Cold Regi. Sci. Tech.*, 17, 83-88.
- Makkonen, L., (2000). Models for the growth of rime, glaze, icicles and wet snow on structures. *Phil. Trans. R. Soc. Lond. A*, 358, 2913-2939.
- Makkonen, L., (2010). Solid fraction in dendritic solidification of a liquid. *Applied Physics Letters*, 96 (9), 091910.
- Marine Science site. Available at: <http://www.marinebio.net/marinescience/02ocean/swcomposition.htm>
- Myers, T.G., and Hammond, D.W., (1999). Ice and water film growth from incoming supercooled droplets. *Int. J. Heat Mass Transfer*, 42, 2233-2242.
- Myers, T.G., (2001). Extension to the messenger model for aircraft icing. *AIAA J.*, 39 (2), 211-218.
- Myers, T.G., Charpin, J.P.F., and Chapman, S.J., (2002). The flow and solidification of a thin fluid film on an arbitrary three dimensional surface. *Phys. Fluids*, 14 (8), 2788-2803.

- Myers, T.G., and Charpin, J.P.F., (2004). A mathematical model for atmospheric ice accretion and water flow on a cold surface. *Int. J. Heat Mass Transfer*, 47, 5483-5500.
- Ono, N., (1967). Specific Heat and Fusion of Sea Ice. in Physics of Snow and Ice: International Conference on Low Temperature Science, edited by H. Oura, *Inst. of Low Temp. Sci.*, Hokkaido Uni., Sapporo, Japan, 1 (1), 599-610.
- Panov, V.V., (1976). Icing of ships. Arkticheskii i Antarkticheskii Nauchno-Issledovatel'skii Institut, *Trudy* 334. *Gidrometeoizdat*, Leningrad, (263 pp). (in Russian)
- Pringle, D.J., Eicken, H., Trodahl, H.J., and Backstrom, L.G.E., (2007). Thermal conductivity of landfast Antarctic and Arctic sea ice. *Journal of Geophysical Research*, C04017, 112, 1-13.
- Ranz, W.E., and Marshal, W.R., (1952). Evaporation from drops-part II. *Chemical Engineering Program*, 48, 173-180.
- Rohsenow, W.M., and Choi, H.Y., (1961). *Heat, Mass, and Momentum Transfer*. Prentice-Hall, Inc.
- Ryerson, C.C., (1995). Superstructure spray and ice accretion on a large US Coast Guard Cutter. *Atmos. Res.*, 36, 321-337.
- Ryerson, C.C., and Gow, A.J., (2000). Crystalline structure and physical properties of ship superstructure spray ice. *Phil. Trans. R. Soc. Lond. A*, 358, 2847-2871.
- Ryerson, C.C., (2011). Ice protection of offshore platforms. *Cold Regi. Sci. Tech.*, 65 (1), 97-110.
- Schröder Hansen, E., (2012). Numerical modeling of marine icing on offshore structures and vessels. *MS thesis*, Department of Physics, Norwegian University of Science and Technology, Norway.
- Schwerdtfeger, P., (1963). The thermal properties of sea ice. *J. Glaciol.*, 4 (36), 789-807.
- Shekhtman, A.N., (1968). The Probability and Intensity of the Icing up of Ocean Going Vessels. *Moskow Nauk-Issled Inst. Aeroklim, T. Vyp*, 50, 55-65.
- Shellard, H.C., (1974). The meteorological aspects of ice accretion on ships. *World Meteorological Organization, Marine Science Affairs*, Report No. 10 (WMO-0No. 397), (34 pp).
- Stallabrass, J.R., (1980). Trawler icing. *A compilation of work done at N.R.C. Mechanical Engineering*, Report MD-56, N.R.C. No. 19372.
- Szilder, K., Lozowski, E.P., and Forest, T.W., (1995). One-dimensional freezing of seawater in a constrained volume. *Can. J. Geotech.*, 32 (1), 122-127.

Tabata, T., Iwata, S., and Ono, N., (1963). Studies on the ice accumulation on ships I. *Low Temperature Science, Series A, Physical Sciences*, 21, 173-221.

Tabata, T., (1969). Studies on the ice accumulation on ships III. *Low Temperature Science, Series A, Physical Sciences*, 27, 339-349.

Tracy, C.R., Welch, W.R., and Porter, W.P., (1980). Properties of air, a manual for use in biophysical ecology. *Third edition, Technical report No. 1*, University of Wisconsin.

US Navy, (1988). Cold weather handbook for surface ships. *OPNAV P-03C-01-89, Chief of Naval Operations*, Washington DC, UAS.

Zakrzewski, W.P., (1986). Icing of ships, Part I: Splashing a ship with spray. *NOAA Technical Memorandum, ERL PMEL-66*, Seattle, USA, (74 pp).

Zakrzewski, W., (1987). Splashing a ship with collision-generated spray. *Cold Regi. Sci. Tech.*, 14 (1), 65-83.

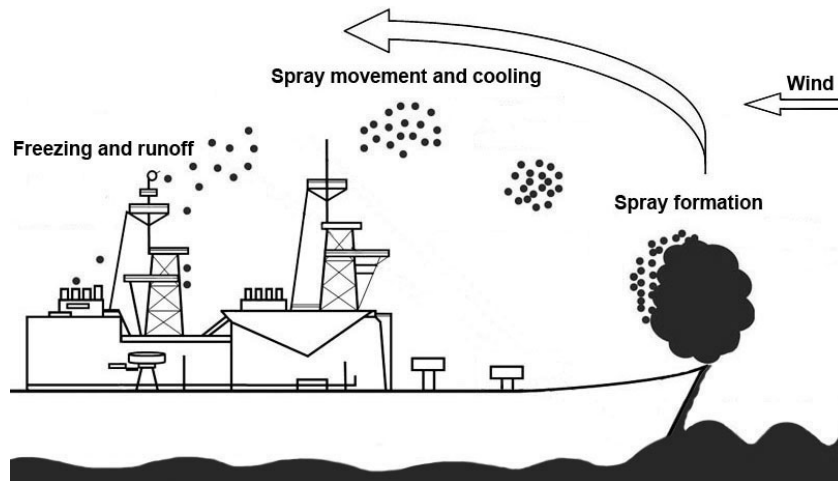


Fig. 1. Schematic of the formation and movement of a spray cloud on a marine vessel (Dehghani-Sanij et al., 2015, 2016)

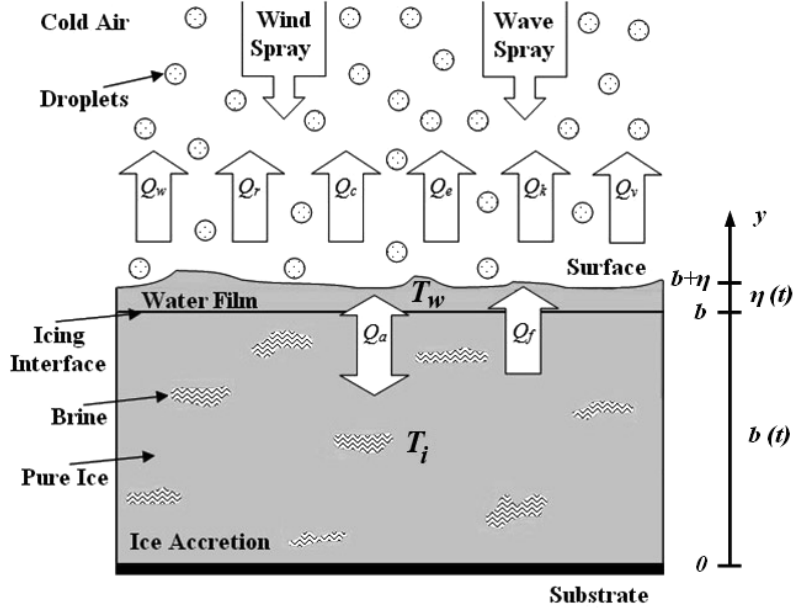


Fig. 2. Schematic illustration of the proposed model

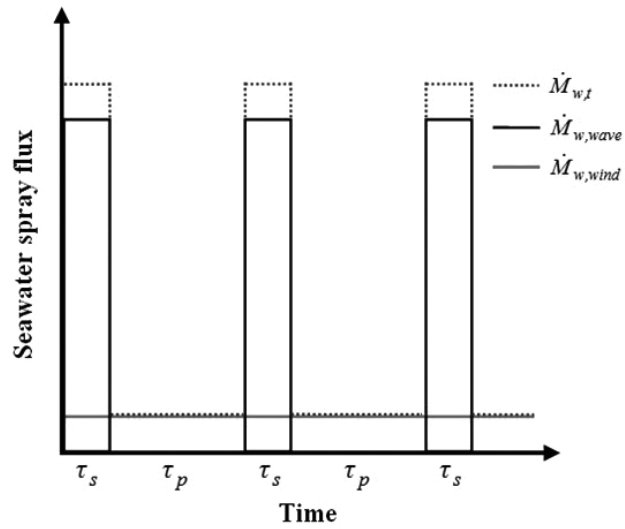


Fig. 3. Schematic illustration of the distribution of seawater spray mass flux during the sea spray events

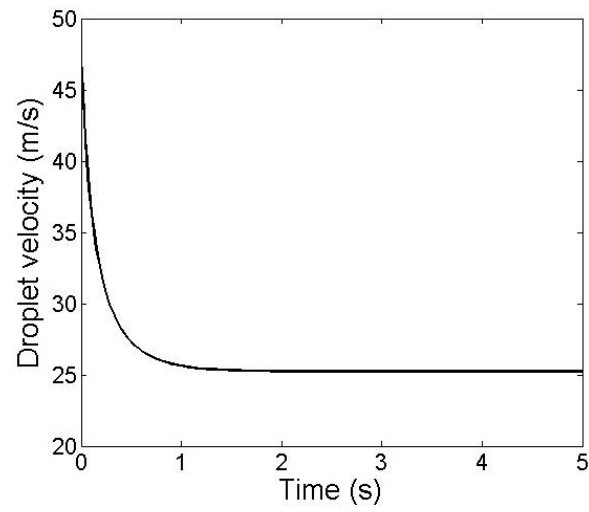


Fig. 4. Variations of the droplet velocity versus time at $U = 20.6 \text{ m/s}$ and $D = 1.5 \text{ mm}$

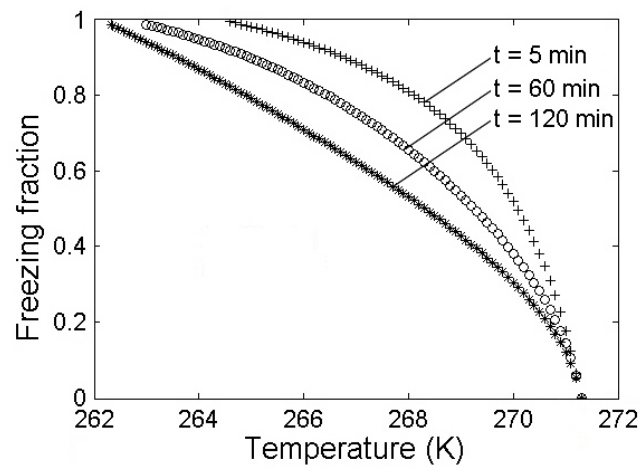


Fig. 5. Variations of the freezing fraction versus air temperature at three different times

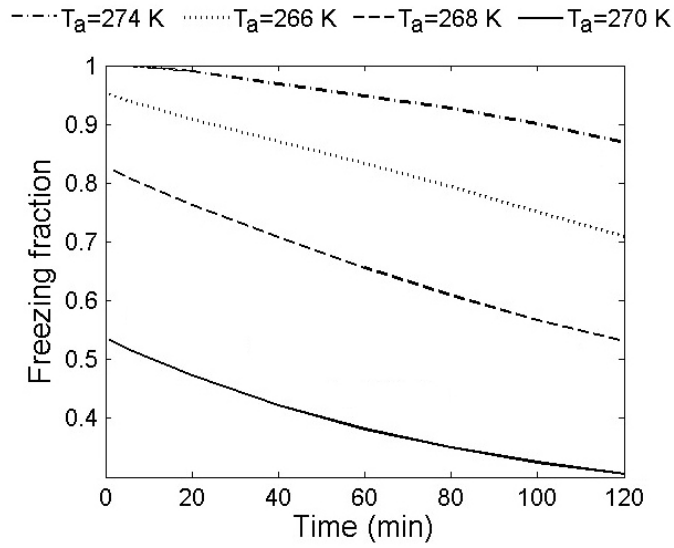


Fig. 6. Variations of the freezing fraction versus time for several air temperatures

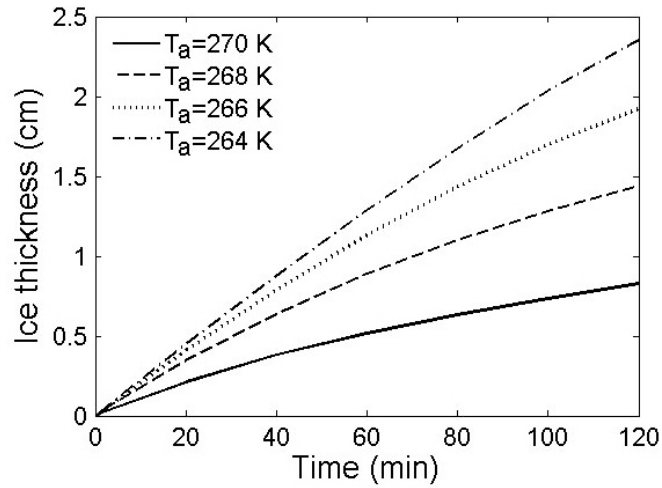


Fig. 7. Variations of the ice formation thickness versus time at different air temperatures

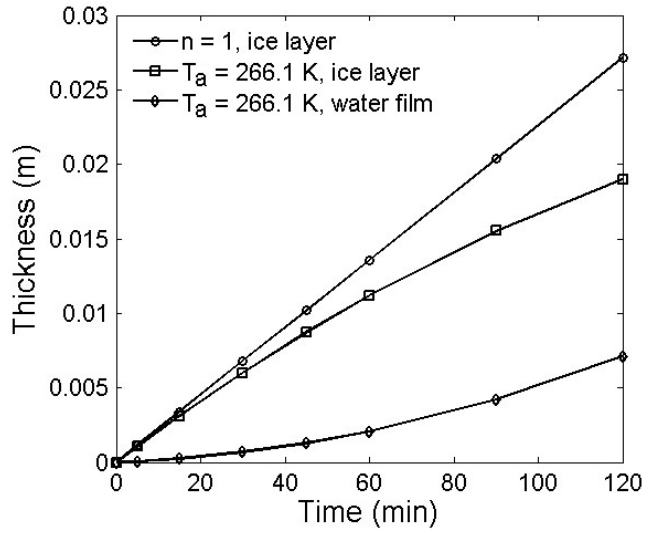


Fig. 8. Variations of the ice layer and water film thicknesses for rime and glaze icing

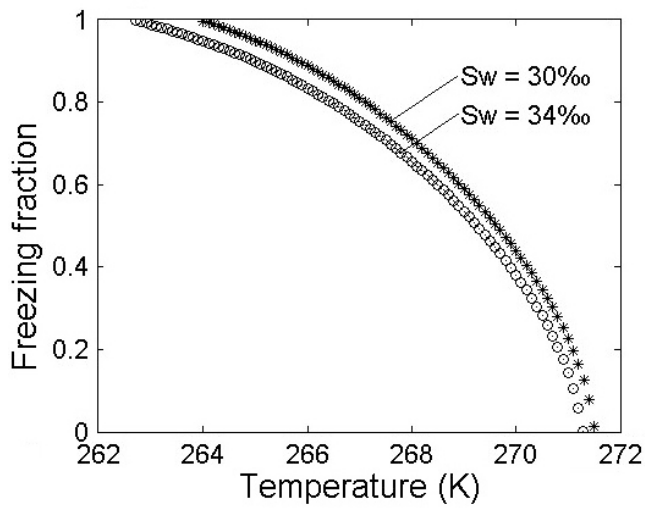


Fig. 9. Variations of freezing fraction versus air temperature at two different salinities

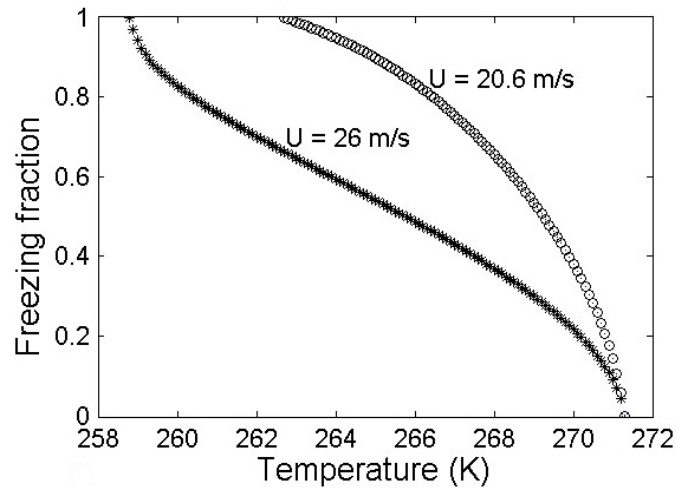


Fig. 10. Variations of freezing fraction versus air temperature at two different wind velocities

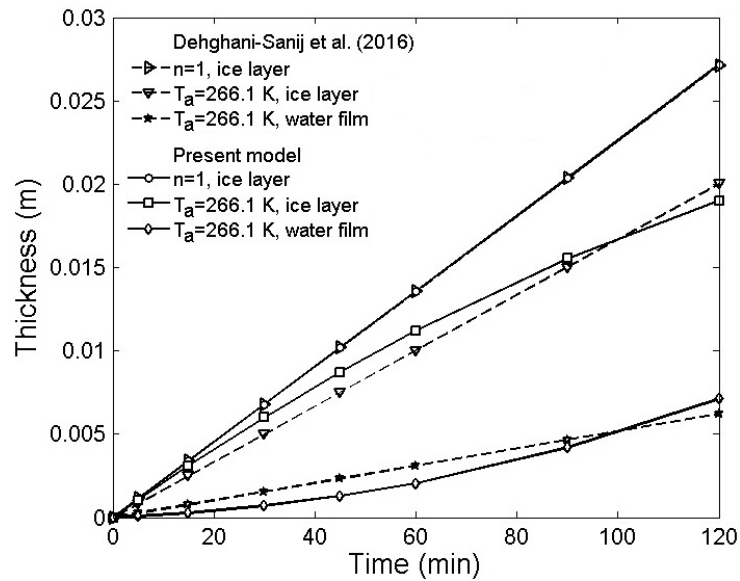


Fig. 11. Comparison of ice layer and water film thicknesses for different models

Table 1. Parameter values

Parameter	Value	Parameter	Value
a	$8.1 \times 10^7 \text{ K}^3$ (Lozowski et al., 2000; Chung and Lozowski, 2010)	RH	80%
B_s	1 for plate (Makkonen, 1987; Horjen, 1983)	S_w	34‰
c_a	1005 $J/kg.K$ (Tracy et al., 1980; Eng. Toolbox, 2016)	$T_{w,i}^{**}$	2 °C
c_w	$\approx 3.93 \times 10^3 \text{ J/kg.K}$ (Schröder Hansen, 2012)	U	20.6 m/s (Borisenkov and Panov, 1972; Lozowski et al., 2000)
D^*	1.5 mm	v_s	12.9 m/s (Lozowski et al., 2000)
D_{ab}	$0.26 \times 10^{-4} \text{ m}^2/s$ (Ranz and Marshal, 1952)	x	20 m
f_s	1 (Jones and Andreas, 2012)	z	10 m
H_{bow}	4 m	α	0° (Lozowski et al., 2000)
k	0.40 (Kulyakhtin and Tsarau, 2014)	α_a	$\approx 15.67 \times 10^{-6} \text{ m}^2/s$ (Eng. Toolbox, 2016)
k_a	0.0243 $W/m.K$ (Eng. Toolbox, 2016)	β	1/3 (Horjen, 2013, 2015)
L	1 m	γ	180°
l_f	$3.34 \times 10^5 \text{ J/kg}$ (Green and Perry, 2008)	ε	0.622 (Kato, 2012; Makkonen, 1989)
l_v	$2.27 \times 10^6 \text{ J/kg}$ (Green and Perry, 2008)	ρ_w	$\approx 1027 \text{ kg/m}^3$ (Schröder Hansen, 2012)
P	10^5 Pa	σ	$5.67 \times 10^{-8} \text{ W/m}^2.K^4$

* Droplet diameter of wave spray

** The temperature of seawater-surface is generally between -1.7 and 5 °C (Environment and Climate Change, Met 101)

Table 2. Variations of air temperature and thickness of ice layer at different times for rime icing

Time (min)	Air temperature (K)	Ice layer thickness (mm)
5	264.4	1.13
15	263.9	3.39
30	263.3	6.79
45	262.9	10.18
60	262.6	13.57
90	262.2	20.35
120	261.9	27.16

Table 3. Variations of the freezing fraction and ice layer and water film thicknesses for glaze icing at $T_a=266.1 K$

Time (min)	Freezing fraction	Ice layer thickness (mm)	Water film thickness (mm)
5	0.9354	1.057	0.064
15	0.9129	3.094	0.259
30	0.8836	5.991	0.691
45	0.8557	8.702	1.286
60	0.8268	11.21	2.058
90	0.7644	15.55	4.200
120	0.7006	19	7.114